

Gamma-Ray and Fast Neutron Shielding Parameters of Two New Titanium-Based Bulk Metallic Glasses

Oyeleke Olarinoye^{1*}, Celestine Oche¹

1. Department of Physics, Federal University of Technology Minna, Nigeria

| ARTICLE INFO | ABSTRACT |
|--|---|
| <p>Article type: Original Paper</p> <p>Article history: Received: Aug 21, 2019 Accepted: Jan 18, 2020</p> <p>Keywords: Glass Photons Fast Neutrons Radiation Lead</p> | <p>Introduction: Low-density bulk metallic glass (BMG) with good structural characteristics has the potential of being used for structural radiation shielding purposes. This study was conducted on two new low-density titanium (Ti)-based BMGs (i.e., $Ti_{32.8}Zr_{30.2}Ni_{5.3}Cu_9Be_{22.7}$ and $Ti_{31.9}Zr_{33.4}Fe_4Cu_{8.7}Be_{22}$) to investigate their photon and fast neutron shielding capacities.</p> <p>Material and Methods: The mass attenuation coefficients, half-value layers, effective atomic numbers, and exposure buildup factors of the two BMGs were calculated at the photon energy values of 15 keV and 15 MeV. Computation of mass attenuation coefficients and effective atomic numbers was accomplished using the XCOM and auto-Z_{eff} software, respectively. In addition, the geometric progression procedure-based computer code EXABCal was used for calculating the exposure buildup factors of BMG. The fast neutron removal cross-sections were also calculated for the two BMGs. The calculated photon and fast neutron shielding parameters for BMGs were compared with those of lead (Pb), heavy concrete, and some recently developed glass shielding materials and then analyzed according to their elemental compositions.</p> <p>Results: The results showed that though Pb had a better photon shielding capacity, Ti-BMG attenuated photons better than heavy concrete. Furthermore, BMG had a higher neutron removal cross-section, compared to heavy concrete and some recently developed glass shielding materials. The neutron removal cross-sections of $Ti_{32.8}Zr_{30.2}Ni_{5.3}Cu_9Be_{22.7}$ and $Ti_{31.9}Zr_{33.4}Fe_4Cu_{8.7}Be_{22}$ were obtained as 0.1663 and 0.1645 cm^{-1}, respectively.</p> <p>Conclusion: his study revealed that Ti-based BMG with high strength and low density have potential applications in high-radiation environments, particularly in nuclear engineering for source and structural shielding.</p> |

► Please cite this article as:

Olarinoye IO, Oche CO. Gamma-Ray and Fast Neutron Shielding Parameters of Two New Titanium-Based Bulk Metallic Glasses. Iran J Med Phys 2021; 18: 139-147. 10.22038/ijmp.2020.42684.1635.

Introduction

The quest for reducing energy consumption and operational cost has encouraged material scientists and engineers to investigate low-density structural materials. Consequently, low-density materials with superior mechanical and physical properties [1-5] have always been a subject of active research in the material science community. Bulk metallic glasses (BMGs) are among such novel materials, which have attracted much interest. These are metallic alloys having an amorphous atomic arrangement obtained by rapid cooling from a high temperature [5]. The amorphous nature of BMGs gives them a high yield strength (above 2 GPa) [6-9]. Furthermore, BMGs exhibit other interesting properties, such as low stiffness, high hardness, low surface roughness, low shrinkage during casting, and high corrosion resistance [1-4, 10]. These properties have encouraged the use of different BMGs in biomedical, automobile, defense, and aerospace industries [11-14]. However, the deployment of many BMGs for these applications has been hindered by their low glass-forming ability (GFA). Consequently, the improvement

of the GFA of metallic alloys has led to the design of BMG alloy compositions based on empirical rules [5, 15-19].

In structural engineering, Ti-based BMGs are currently the most suitable low-density BMGs [5, 10]. This is due to their low densities (4-7 gcm^{-3}), high strength and toughness, fabrication ease (due to low-temperature requirement), high mechanical properties (similar to crystalline Ti), and low production cost. Accordingly, recent research has improved the GFA of Ti-based BMG [5]. Recently, two Ti-based BMGs, namely $Ti_{32.8}Zr_{30.2}Ni_{5.3}Cu_9Be_{22.7}$ (T1) and $Ti_{31.9}Zr_{33.4}Fe_4Cu_{8.7}Be_{22}$ (T2), [16, 19] with a high compressive fracture strength (about 1800 MPa) and a GFA greater than 50 have been reported. These materials were adjudged to be good materials in structural engineering applications. The potential use of these materials for structural engineering applications also suggests that they may be good options for structural radiation shield. The beryllium content of the BMG also suggests that they may be good material for fast neutron absorber.

*Corresponding Author: Tel: +2347067533885, Email: leke.olarinoye@futminna.edu.ng

Traditionally, structural radiation shielding materials include high-density concrete and lead (Pb). The poisonous nature of Pb has limited its application for this purpose. On the other hand, concrete suffers from cracking and unstable properties due to temperature changes leading to the alteration of its hydrogen content [20]. Consequently, a tough material with lower density, compared to that of Pb, such as Ti-based BMG, would be a potentially good alternative for radiation shielding purposes. Furthermore, the application of Ti-based BMG may extend to radiation environments, such as space. Regarding this, it is required to study the radiation interaction processes of the material. To the best of our knowledge, the study of the radiation shielding capacity of Ti-based BMG is very scarce in the literature.

The present study was conducted to evaluate the fast neutron and photon shielding parameters of $\text{Ti}_{32.8}\text{Zr}_{30.2}\text{Ni}_{5.3}\text{Cu}_9\text{Be}_{22.7}$ (T1) and $\text{Ti}_{31.9}\text{Zr}_{33.4}\text{Fe}_4\text{Cu}_{8.7}\text{Be}_{22}$ (T2) in order to determine their suitability for structural shielding purposes. To this end, the mass attenuation coefficient, half-value layer (HVL), effective atomic number (Z_{eff}), exposure buildup factor (EBF) at the photon energies of 15 keV to 15 MeV, and macroscopic effective removal cross-section of the fast neutron of T1 and T2 were calculated and then compared to those of Pb and heavy concrete.

Materials and Methods

Two Ti-based BMGs (i.e., T1 and T2) were considered for their photon and fast neutron shielding effectiveness in this study. The BMGs were prepared by pure melting elemental compositions of BMG according to previous research [16, 19]. Photon and fast neutron shielding parameters of two new Ti-based BMGs (i.e., T1 and T2) were theoretically evaluated and presented in this study. The photon shielding capacity of BMG was assessed via the mass attenuation coefficients (μ_m), HVL, and EBF, while the fast neutron removal cross-section (FNRCs) was used to assess the fast neutron shielding efficacy. In addition, their radiation shielding capacities were compared to those of heavy concrete (StMg), Pb, and some recently developed glass materials for shielding, namely $80\text{TeO}_2\cdot 20\text{B}_2\text{O}_3$ (TeBO), $80\text{TeO}_2\cdot 20\text{WO}_3$ (TeWO), and $60\text{PbO}\cdot 40\text{P}_2\text{O}_5$ (PbBO) [21, 22]. The chemical compositions (by weight %) of the considered heavy concrete were as follows: H=0.51, O=15.70, Mg=0.58, Al=0.66, Si=2.68, P=0.08, S=0.06, Ca=3.95, Mn=0.07, and Fe=75.73. Furthermore, the density of this material was 5.11 g/cm^3 [21]. The densities of TeBO, TeWO, and PbBO glasses were 4.97, 5.95, and 6.74 g/cm^3 , respectively.

Theoretical Background of Shielding Parameters Mass Attenuation Coefficient

When a beam of monochromatic photons is incident on a thin absorbing medium of mass thickness t , the intensity is reduced on emerging from the medium according to Equation (1):

$$I = I_0 e^{-\mu_m t} \quad (1)$$

where I , I_0 , and μ_m are the transmitted photon intensity (attenuated), incident photon intensities, and mass attenuation coefficient of the material medium, respectively. The μ_m measures the mean number of photo-interactions between the incident photons and the absorbing medium at a given mass thickness. The μ_m can be used to compare the photon shielding capacity of different material at specific photon energy. It can be experimentally determined using Equation (1) or theoretically through the use of computer codes, such as MCNP5 and XCOM [23, 24]. For composite material, μ_m is estimated using the mixture rule based on Equation (2) [25]:

$$\mu_m^c = \sum_i^n w_i \mu_m^i \quad (2)$$

where μ_m^c , μ_m^i , and w_i are the mass attenuation coefficients of the composite material, and i^{th} component in the material, and weight fraction of the i^{th} component of the composite material, respectively. The XCOM computer code was used to evaluate the mass attenuation coefficients of T1 and T2 and then compare them with those of StMg and Pb.

Half-Value Layer

The HVL is the thickness of an absorbing material required to reduce the density of an incident photon of specific energy by 50%. The HVL is calculated from the mass attenuation coefficient according to Equation (3):

$$\text{HVL} = 0.693 / \rho \mu_m \quad (3)$$

The HVL can also be used as a quantity to describe the relative shielding capacity of different shielding materials. Equation 3 was used for estimating the HVLs of T1 and T2. These values were compared with those of StMg and Pb.

Effective Atomic Number (Z_{eff})

Many of the photon interaction modes depend on the atomic number (Z) of the interacting medium. Though many of the materials used in many photon applications are composite materials containing more than one pure element, the effective atomic number is a convenient parameter used similarly to represent its atomic number as if it was a pure element. Unlike Z , Z_{eff} is not a constant over all photon energies; it varies depending on the comparative importance of photon interaction processes [26, 27]. The Z_{eff} is an important parameter for radiation dose measurement and shielding calculations [26]. The effective atomic number can be estimated using Equation (4) [27]:

$$Z_{\text{eff}} = \frac{\sum_i f_i A_i (\mu_m)_i}{\sum_j f_j \frac{A_j}{Z_j} (\mu_m)_j} \quad (4)$$

where f_i , A_i , and Z_i are the fractional abundance, atomic weight, and atomic number of element i , respectively.

Exposure Buildup Factor

The experimental determination of mass attenuation coefficients of materials via Equation 1 requires a thin absorber, as well as a monochromatic and well-collimated photon beam. For many practical applications, radiation shields are not thin, and photons may not be monochromatic and collimated. Consequently, Equation 1 is always modified to account for multiple-photon scattering and buildup in the thick absorber. The buildup factor (B) accounts for the ratio of the broad beam to that of a collimated beam and directly influences radiation absorption for absorbed dose or shielding calculations.

The American Nuclear Society provided the data related to the photon buildup factors of 23 elements (i.e., Be, B, C, N, O, Na, Mg, Al, Si, P, S, Ar, K, Ca, Fe, Cu, Mo, Sn, La, Gd, W, Pb, and U), one compound (i.e., water), and two mixtures (i.e., air and ordinary concrete) for the standard photon energies of 0.015-15 MeV and penetration depth of up to 40 mean free path (mfp) [28]. These data are usually used as a standard for estimating buildup factors for undefined substances via the geometric progression (GP) fitting method [29-33]. The evaluation of buildup factors using the GP method requires three distinct procedures described in the next sections.

Calculation of equivalent atomic number

Calculation of equivalent atomic number (Z_{eq}) for any material can be accomplished by estimating the Compton partial interaction coefficient (μ_c) and mass attenuation coefficients (μ_m) at a photon energy range of 0.015-15 MeV using the XCOM software. The ratio $R = \mu_c/\mu_m$ of each material is then calculated and matched at the standard energies to the corresponding ratios of elements up to the heaviest element. If the value of the ratio matches that of any of the elements, then the atomic number of that element becomes the equivalent atomic number of the material. However, if the value of R obtained for the considered material does not match that of any element but rather falls between the ratios of two successive elements, then the Z_{eq} of such material is interpolated using Equation (5) [29-32]:

$$Z_{eq} = \frac{Z_1(\log R_2 - \log R) + Z_2(\log R - \log R_1)}{\log R_2 - \log R_1} \quad (5)$$

Here, R_1 and R_2 are the ratios (μ_c/μ_m) of the two successive elements of atomic numbers Z_1 and Z_2 , respectively, within which R falls at each energy.

Evaluation of geometric progression fitting parameters

Evaluation of photon buildup factors by the GP fitting method requires five fitting parameters [29, 30]. These parameters (i.e., b , c , a , X_k , and d) depend on Z_{eq} and photon energy. The GP fitting coefficients of the material is also interpolated using the logarithmic interpolation formula:

$$P = \frac{P_1(\log Z_2 - \log Z_{eq}) + P_2(\log Z_{eq} - \log Z_1)}{\log Z_2 - \log Z_1} \quad (6)$$

where P_1 and P_2 are the GP fitting parameters obtained from the ANS database corresponding to the atomic numbers Z_1 and Z_2 , respectively.

Estimation of exposure buildup factor

The EBFs ($EBF(E, x)$) for a given material is estimated based on the fitting parameters for the given incident energy (E) in the spectrum (0.015-15 MeV) at different penetration depths (x) up to 40 mfp by Equations (7), (8), and (9) [29, 30]:

$$EBF(E, x) = 1 + \frac{(b-1)(K^x-1)}{K-1}, \text{ for } K \neq 1 \quad (7)$$

$$EBF(E, x) = 1 + (b-1)x, \text{ for } K = 1 \quad (8)$$

$$K(E, x) = cx^a + d \frac{\tanh(x/X_k - 2) - \tanh(-2)}{1 - \tanh(-2)} \text{ for } x \leq 40 \text{ mfp} \quad (9)$$

The EBFs of the considered materials were evaluated using a window-based computer code EXABCal [33], which utilizes the GP fitting procedure in its configuration.

Fast neutron effective removal cross-section

The attenuation of fast neutrons through a material medium can be estimated using its effective removal cross-section also referred to as the macroscopic removal cross-section. The FNRCS (Σ_R) is a measure of the probability that a neutron will undergo specific interactions per unit length of the material it traverses through [34]. The Σ_R has been developed to accommodate neutron scattering and buildup. For composite material, the Σ_R is often estimated via Equation (10) [21]:

$$\Sigma_R = \sum w_i \left(\frac{\Sigma_R}{\rho} \right)_i \quad (10)$$

where w_i and $\left(\frac{\Sigma_R}{\rho} \right)_i$ are the partial density and mass removal cross-section of the i^{th} component of the composite material, respectively. The values Σ_R/ρ are fairly constant for neutron energies of 2-12 MeV [35, 36]. To theoretically calculate Σ_R of the two Ti-BMG and StMg (heavy) concrete using Equation (10), the Σ_R/ρ of each of the elements in each compound/mixture was obtained from the literature [37, 38], and the partial density of each elemental constituent was evaluated using their weight fractions in each compound/mixture [21]. For each element in a compound/mixture, the partial density w_i of each elemental composition in a material was evaluated through Equation (11):

$$w_i = m_i \rho \quad (11)$$

where m_i is the weight fraction of the i^{th} element in the material of ρ density. The validity of Equation (10) has been reported to be accurate within 10% of experimental values.

Results

Figure 1 displays the μ_m of T1, T2, and two traditional shielding materials (i.e., Pb and StMg) at the energy range of 0.015-15 MeV obtained theoretically from the XCOM code. At the lowest end of the considered energy spectrum (0.015 MeV), the values of μ_m were 29.7, 28.5, 112, and 45.1 cm^2/g for T1, T2, Pb, and StMg, respectively. On the other hand, at the peak of the energy spectrum, μ_m values for the mentioned materials were obtained as 0.0285, 0.0287, 0.0566, and 0.0285 cm^2/g , respectively. The μ_m of T1, T2, and three recently developed shielding glasses are presented in Figure 2 for comparison purposes.

Figure 3 illustrates the variations in the HVL of the materials considered in this study at the given energies. Within the energy spectrum of interest in this study, the HVL of StMg was at the highest level, while that of Pb was at the lowest level. The HVLs of the materials at the lowest energy were 4.20×10^{-3} , 4.37×10^{-3} , 54.80×10^{-3} , and 3.07×10^{-3} cm for T1, T2, Pb, and StMg, respectively.

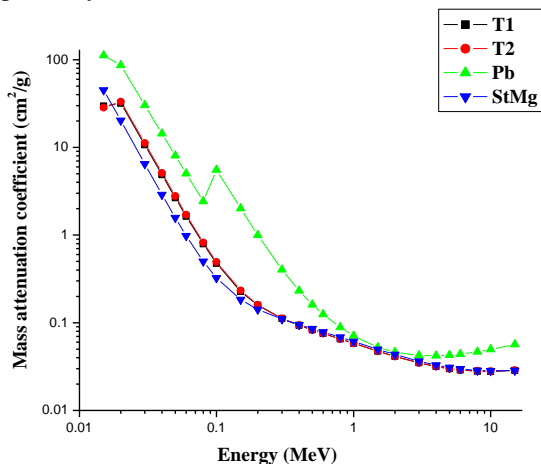


Figure 1. Mass attenuation coefficients of T1, T2, lead, and heavy concrete

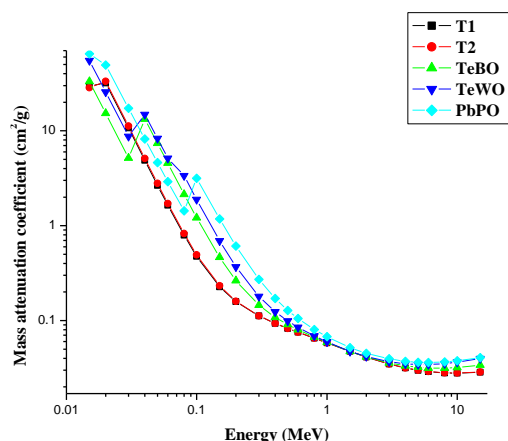


Figure 2. Mass attenuation coefficients of T1, T2, compared to those of TeBO, TeWO, and PbPO

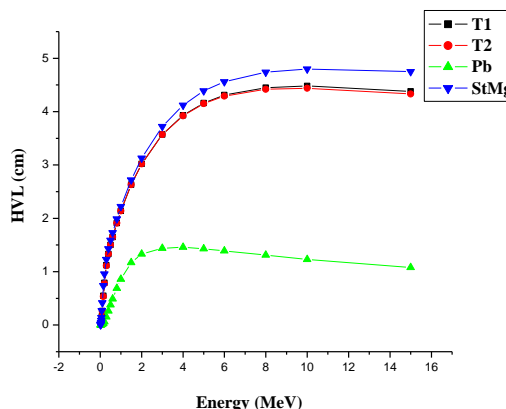


Figure 3. Half-value layers of T1, T2, lead, and heavy concrete as a function of photon energy

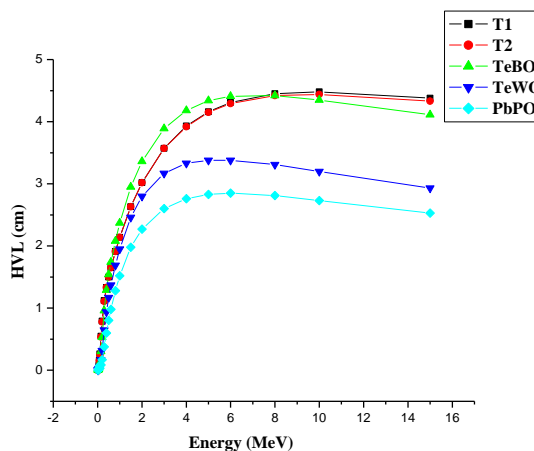


Figure 4. Half-value layers of T1, T2, TeBO, TeWO, and PbPO as a function of photon energy

In addition, at a photon energy of 15 MeV, the HVLs were obtained as 4.38, 4.33, 1.08, and 4.75 for T1, T2, Pb, and StMg, respectively. The HVLs of T1 and T2 were approximately equal, and their values lay between those of Pb and StMg for energies (E) greater than 3 MeV. At the energy of < 3 MeV, the HVLs of T1, T2, and StMg were almost equal. Figure 4 depicts the comparison of the HVLs of T1 and T2 with those of TeWO, TeBO, and PbBO.

The Z_{eff} of the Ti-BMG was evaluated using the Auto- Z_{eff} software [37], and the results are presented in Table 1 at the photon energy range of 0.015-15 MeV. At the lowest energy, T1 and T2 had the Z_{eff} value of 17.97 and 17.88, respectively. On the other hand, at the peak energy, the Z_{eff} values were estimated at 15.32 and 15.65 for T1 and T2, respectively. Furthermore, the maximum values of the effective atomic number for T1 and T2 at a photon energy of 0.05 MeV were 23.17 and 23.59, respectively. The Z_{eff} values generally increased from 15 keV to 50 keV, thereafter it decreased steadily up to 1.5 MeV before it started to increase again.

Table1. Effective and equivalent atomic numbers (equations 4 and 5) and geometric progression fitting parameters (equation 6) of T1 and T2

| E (MeV) | T1 | | | | | | | T2 | | | | | | |
|---------|------------------|-----------------|---------|---------|---------|----------------|---------|------------------|-----------------|---------|---------|---------|----------------|---------|
| | Z _{eff} | Z _{eq} | b | c | a | X _k | d | Z _{eff} | Z _{eq} | b | c | a | X _k | d |
| 0.015 | 17.97 | 20.72 | 1.00646 | 0.76976 | -0.0825 | 6.77252 | 0.16922 | 17.88 | 20.71 | 1.0066 | 0.72449 | -0.0556 | 6.83959 | 0.15875 |
| 0.02 | 22.61 | 28.44 | 1.00997 | 0.11177 | 0.71725 | 10.978 | -0.9168 | 23.01 | 28.44 | 1.00953 | 0.10781 | 0.73835 | 10.8887 | -0.982 |
| 0.03 | 23.01 | 29.25 | 1.02066 | 0.36024 | 0.20376 | 13.4312 | -0.073 | 23.41 | 29.27 | 1.08498 | 0.37726 | 0.20263 | 12.606 | -0.0574 |
| 0.04 | 23.17 | 29.89 | 1.11469 | 0.33038 | 0.23418 | 14.8541 | -0.0961 | 23.57 | 29.88 | 1.26869 | 0.33122 | 0.22368 | 15.7346 | -0.0959 |
| 0.05 | 23.17 | 30.32 | 1.19551 | 0.33247 | 0.21243 | 13.1273 | -0.1284 | 23.59 | 30.31 | 1.29807 | 0.31149 | 0.18724 | 13.3227 | -0.1182 |
| 0.06 | 23.07 | 30.63 | 1.10103 | 0.38221 | 0.22619 | 13.6083 | -0.1269 | 23.50 | 30.62 | 1.09666 | 0.39221 | 0.22025 | 13.6458 | -0.1225 |
| 0.08 | 22.57 | 31.08 | 1.17186 | 0.43149 | 0.20347 | 13.8594 | -0.1196 | 23.04 | 31.08 | 1.16576 | 0.42632 | 0.20755 | 13.8201 | -0.1232 |
| 0.1 | 21.73 | 31.39 | 1.2568 | 0.48439 | 0.17934 | 13.7399 | -0.1044 | 22.23 | 31.41 | 1.24848 | 0.47816 | 0.18329 | 13.6985 | -0.1078 |
| 0.15 | 18.68 | 31.88 | 1.4584 | 0.62917 | 0.11979 | 13.7727 | -0.0678 | 19.25 | 31.89 | 1.44689 | 0.62032 | 0.12362 | 13.7307 | -0.0701 |
| 0.2 | 16.04 | 32.21 | 1.60653 | 0.773 | 0.07258 | 13.8675 | -0.0455 | 16.54 | 32.22 | 1.5925 | 0.76316 | 0.07585 | 13.9068 | -0.0469 |
| 0.3 | 13.67 | 32.84 | 1.76661 | 0.93706 | 0.02841 | 13.0849 | -0.0301 | 14.04 | 32.81 | 1.75429 | 0.92629 | 0.03134 | 13.1569 | -0.0314 |
| 0.4 | 12.88 | 33.35 | 1.82156 | 1.04006 | 0.00412 | 12.3686 | -0.0216 | 13.19 | 33.35 | 1.81215 | 1.02971 | 0.00653 | 12.4676 | -0.0225 |
| 0.5 | 12.55 | 33.8 | 1.83682 | 1.09587 | -0.0088 | 11.5581 | -0.0169 | 12.84 | 33.77 | 1.82961 | 1.08657 | -0.0068 | 11.7217 | -0.0176 |
| 0.6 | 12.37 | 34.1 | 1.83244 | 1.12877 | -0.0163 | 10.7646 | -0.0149 | 12.65 | 34.08 | 1.82709 | 1.12052 | -0.0145 | 10.9759 | -0.0155 |
| 0.8 | 12.21 | 34.4 | 1.80866 | 1.14336 | -0.0212 | 9.93533 | -0.0129 | 12.47 | 34.44 | 1.80523 | 1.13596 | -0.0198 | 10.1953 | -0.013 |
| 1 | 12.13 | 34.47 | 1.78428 | 1.14186 | -0.0218 | 10.1687 | -0.0121 | 12.39 | 34.55 | 1.78148 | 1.13638 | -0.0208 | 10.4064 | -0.0121 |
| 1.5 | 12.10 | 32.15 | 1.71228 | 1.16823 | -0.0335 | 16.9024 | 0.00786 | 12.35 | 32.25 | 1.70892 | 1.16551 | -0.033 | 16.6659 | 0.00742 |
| 2 | 12.22 | 28.69 | 1.7008 | 1.12168 | -0.021 | 8.58249 | -0.0047 | 12.48 | 28.55 | 1.69744 | 1.12129 | -0.021 | 8.76666 | -0.0044 |
| 3 | 12.62 | 25.91 | 1.62839 | 1.06018 | -0.0056 | 12.1239 | -0.0125 | 12.89 | 25.82 | 1.62734 | 1.05928 | -0.0052 | 12.0223 | -0.013 |
| 4 | 13.04 | 25.17 | 1.55714 | 1.02265 | 0.00539 | 12.7565 | -0.0186 | 13.33 | 25.20 | 1.55549 | 1.02398 | 0.00524 | 12.8255 | -0.0188 |
| 5 | 13.43 | 24.92 | 1.48887 | 1.00289 | 0.0127 | 13.1411 | -0.0252 | 13.73 | 24.95 | 1.48694 | 1.0049 | 0.01247 | 13.1342 | -0.0254 |
| 6 | 13.77 | 24.81 | 1.44639 | 0.97535 | 0.023 | 13.3235 | -0.0342 | 14.07 | 24.78 | 1.4451 | 0.97672 | 0.023 | 13.3372 | -0.0346 |
| 8 | 14.31 | 24.68 | 1.36017 | 0.96531 | 0.02956 | 13.6136 | -0.0407 | 14.62 | 24.64 | 1.35851 | 0.96764 | 0.02941 | 13.6233 | -0.0411 |
| 10 | 14.70 | 24.59 | 1.3016 | 0.94469 | 0.04056 | 13.8636 | -0.0522 | 15.03 | 24.59 | 1.30041 | 0.9458 | 0.04093 | 13.8911 | -0.0532 |
| 15 | 15.32 | 24.59 | 1.20479 | 0.94512 | 0.04929 | 14.2367 | -0.0582 | 15.65 | 24.57 | 1.20331 | 0.94815 | 0.04922 | 14.2708 | -0.0585 |

Table 1 presents the equivalent atomic number and GP fitting parameters of T1 and T2 calculated using Equations (5) and (6) via EXABCal. Figures 5 and 6 display the variation in the EBFs of T1 and T2 at the given photon energy and depth of up to 40 mfp. Figures 7 and 8 show the variation in EBF as a function of depth for the photon energies of 0.15 MeV and 1.5 MeV, respectively.

The Σ_R values of T1, T2, StMg (heavy) concrete, TeWO, TeBO, and PbBO were evaluated by means of Equations (10) and (11) as presented in Figure 9. The Σ_R/ρ values of the elemental make-up of T1, T2, StMg, TeWO, TeBO, and PbBO were obtained from the literature [35, 36, 38]. The Σ_R values were respectively obtained as 0.1663, 0.1645, 0.1420, 0.1204, 0.11, and 0.150 cm⁻¹ for the aforementioned materials.

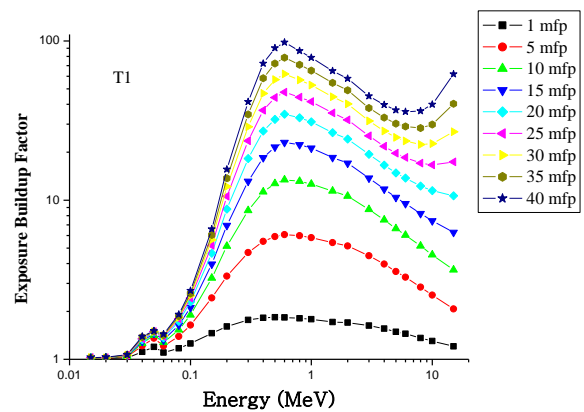


Figure 5. Exposure buildup factors of T1 as a function of energy at different depths (mfp)

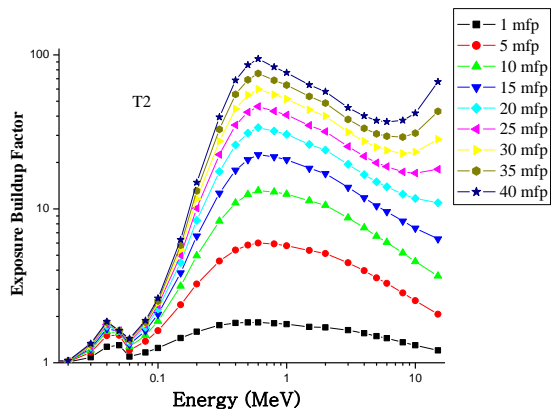


Figure 6. Exposure buildup factors of T2 as a function of energy at different depths (mfp)

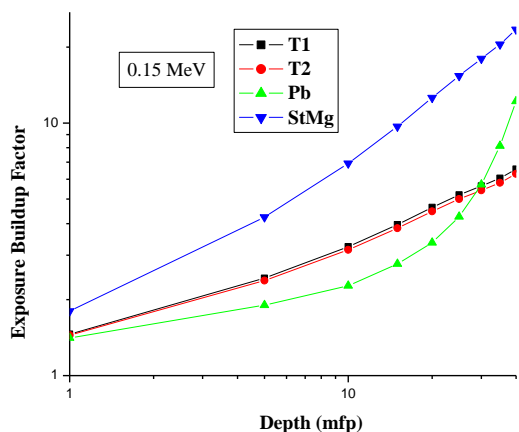


Figure 7. Exposure buildup factors of T1, T2, lead, and heavy concrete as a function of depths (mfp) at 150 keV

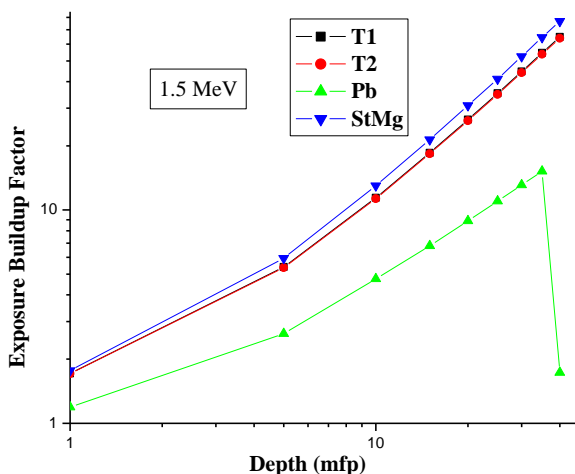


Figure 8. Exposure buildup factors of T1, T2, lead, and heavy concrete as a function of depths at 1.5 MeV

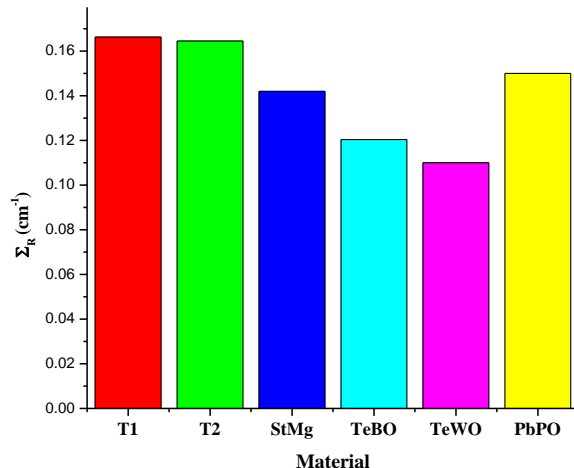


Figure 9. Effective fast neutron removal cross-sections for T1 and T2, compared with those of other materials

Discussion

As the findings revealed, the μ_m values of the four materials under investigation were high for low-photon energies and gradually decreased as the energy increased (Figure 1). This trend is due to the fact that high-energy photons are more penetrating; consequently, μ_m values are lower in this region for all materials. The density of a composite material plays a vital role in its ability to absorb photons at a low energy. This is due to the fact that the dominant interactions at a low energy are dependent on the atomic number and density of the material [21, 31, 34]. Consequently, the relative μ_m of four materials at the energies below 0.1 MeV compares directly with their density and atomic number.

There was no significant difference between the μ_m values of two Ti-based BMGs within this energy range due to the almost equal density of 5.56 and 5.57 g/cm³, respectively. Beyond 0.10 MeV, it appeared that the density had little or no effect on the mass attenuation coefficients of the four materials. This could be attributed to the predominance of pair production effect in this energy region beyond 0.1 MeV which is independent of material density. Although the μ_m values of the two BMGs were lower than that of Pb within the considered energy spectrum, the Ti-based BMGs were still better shielding materials, compared to StMg.

Similarly, the HVL of Pb was at the lowest level, compared to those of T1, T2, and StMg. However, the thickness of Ti-based BMG required for the reduction of photon energies lower than 15 MeV was smaller than that required for StMg (Figure 2). Equation (3) explains the trend observed in Figure 2 as HVL is inversely related to both μ_m and density.

As depicted in Figure 3, the μ_m of T1 and T2 are slightly higher than those of TeWO and TeBO in the lower energy region. However, the μ_m of PbBO, TeWO, and TeBO were higher than those of T1 and T2 in the high-energy region. This is due to the higher concentrations of higher atomic number elements (Te, W, and Pb) in these materials. The higher density of T1

and T2 among the compared materials seemed to have little impact on dictating the mass attenuation coefficients of the materials. On the other hand, high atomic number constituents play a prominent role in dictating the relative μ_m of the materials, especially for higher photon energies.

The HVL of PbPO had the lowest (Figure 4) comparability to those of T1, T2, TeWO, and TeBO. The Pb content of PbBO is chiefly responsible for this issue. The elements with higher atomic numbers provide more electrons to interact with photon beam through the processes of photoelectric effects, as well as coherent and incoherent scattering. These processes eventually lead to the absorption of photons in the medium and consequently a high μ_m . These results showed that the photon shielding capacities of the two Ti-based BMGs were better than that of StMg but inferior to that of Pb. However, the use of BMG as an alternative for Pb in radiation shielding would eliminate the possibility of Pb poisoning.

As indicated in Table 1, it is clear that the Z_{eff} is not constant across the energy spectrum but similarly varies with energy for the two BMGs. The Z_{eff} values were also noticed to lie between the minimum and maximum atomic numbers of the constituents elements (i.e., 4-40). The maximum Z_{eff} was observed at 40 keV with the values of 23.17 and 23.50 for T1 and T2, respectively. In addition, the minimum values of 12.10 and 12.35 were observed at the photon energies of 1.5 MeV for T2 and T1, respectively. The changes of the effective atomic number with energy could be explained based on the partial photon interaction coefficients. For the energy spectrum considered, the photoelectric effect, Compton scattering, and pair production processes were the major partial interaction modes of importance. The photoelectric effect interaction coefficient is dependent on the fifth power of the effective atomic number, while the Compton and pair production interaction coefficients are directly proportional to Z_{eff} and the square of Z_{eff} , respectively [25, 31, 37].

Consequently, the maximum values recorded at a low-energy region could be attributed to the dominance of the photoelectric effect in this region. Conversely, the minimum values of Z_{eff} at 1.5 MeV could be the result of the dominance of the Compton interaction process which has the least dependence on the effective atomic number of the material. At all energies, the Z_{eff} values of T2 were slightly greater than those of T1. This is attributed to the higher concentration of Zr with a high atomic number in T2 (33.4), compared to that in T1 (32.8). This also explains why the mass attenuation of T2 was slightly greater than that of T1.

The variations in EBFs (figures 5 and 6) were similar with respect to energy and depth. It is observed from the figures that EBF values for T1 and T2 are low at lower and higher photon energies but maximum for intermediate energies. This is as a result of the dominance of photoelectric and pair production processes at the lower and higher regions of the energy

spectrum, respectively. Both processes remove photon completely from photon beam, thereby resulting in low photon density (buildup) after interaction. On the other hand, in the intermediate energy region, the Compton (incoherent) scattering dominates the photon interaction mode. Consequently, multiple photon scattering takes place and photon of lower energies are produced; therefore, a high buildup of photons are recorded in this region [25, 37, 39, 40].

The EBFs of T1 and T2 were almost equal at all energies and depth. This could be attributed to their similar elemental compositions and mass attenuation coefficients. The comparison of the EBFs of T1, T2, StMg concrete, and Pb at the selected energies of 150 keV and 1.5 MeV as a function of depth is presented in figures 7 and 8. The figures showed an inverse relationship between the mass attenuation coefficient and the buildup factor. Consequently, the EBF of Pb was at the lowest level, implying better photon shielding capacity, while the EBF of heavy concrete was higher than that of the BMG. Furthermore, at a lower energy (0.15MeV), and for depths greater than 30 mfp, the Ti-based BMG had the lowest EBF; therefore, they are better photon shield, compared to Pb and heavy concrete at this thickness.

The results of FNRCS showed that the Σ_R of the BMG was almost equal with the value for T1 (0.1663 cm^{-1}), which was slightly higher than that of T2 (0.1645 cm^{-1}). This can be attributed to their similar elemental composition. Furthermore, the comparison of these values with those of heavy concrete (0.1420 cm^{-1}), TeWO (0.11 cm^{-1}), TeBO (0.1204 cm^{-1}), and PbBO (0.150 cm^{-1}) revealed that T1 and T2 had superior FNRCS. This result shows that the Σ_R of materials is not a function of their physical density and high-atomic number constituents exclusively, but rather depends on the removal cross-section of individual elements that make up the composite material.

Consequently, the removal cross-sections of T1 and T2 were higher than that of denser PbBO due to the inclusion of Be in their matrix which is an element with high mass neutron removal cross-section, compared to PbBO and other elements in StMg matrix. The high mass neutron removal cross-section for Be can also explain why the Σ_R value of T1 was slightly higher (despite its lower density) than that of T2 since T1 contains slightly higher Be content (22.7%), compared to T2 (22%). Therefore, a high atomic density of high Σ_R elements is a major factor for a good fast neutron absorber. Although the two BMGs contain high-density elements, their Σ_R value could also be attributed to a good balance between high and low atomic number materials. The two new BMGs considered in this study can be concluded to be good absorbers for fast neutrons and potentially good materials for fast neutron moderation.

Conclusion

This study involved the calculation of the mass attenuation coefficients, HVL, effective atomic number,

EBF, and FNRCs of two new Ti-based BMGs (i.e., $Ti_{32.8}Zr_{30.2}Ni_{5.3}Cu_9Be_{22.7}$ and $Ti_{31.9}Zr_{33.4}Fe_4Cu_{8.7}Be_{22}$) at a photon energy range of 15 keV to 15 MeV and comparison of these parameter to those of Pb and heavy concrete (i.e., two traditional shielding materials), as well as three new recently developed glass materials. The study showed that $Ti_{32.8}Zr_{30.2}Ni_{5.3}Cu_9Be_{22.7}$ and $Ti_{31.9}Zr_{33.4}Fe_4Cu_{8.7}Be_{22}$ were superior photon and fast neutron absorbers, compared to heavy concrete. Consequently, it can be concluded that both Ti-based BMGs with high fracture strength and low density can be used for structural shielding purposes, protection of sealed nuclear sources used in medicine and research, and other applications in high-radiation environments,

References

- Chen S, Tu J, Hu Q, Xiong X, Wu J, Zou J, et al. Corrosion resistance and in vitro bioactivity of Si-containing coating prepared on a biodegradable Mg-Zn-Ca bulk metallic glass by micro-arc oxidation. *Journal of Non-Crystalline Solids*. 2017; 456:125-31.
- Inoue A, Takeuchi A. Recent development and application products of bulk glassy alloys. *Acta Materialia*. 2011;59(6):2243-67.
- Li H, Pang S, Liu Y, Sun L, Liaw PK, Zhang T. Biodegradable Mg-Zn-Ca-Sr bulk metallic glasses with enhanced corrosion performance for biomedical applications. *Materials & Design*. 2015; 67:9-19.
- Wang D, Li Y, Sun BB, Sui ML, Lu K, Ma E. Bulk metallic glass formation in the binary Cu-Zr system. *Applied Physics Letters*. 2004; 84(20):4029-31.
- Jiang JZ, Hofmann D, Jarvis DJ, Fecht HJ. Low-Density High-Strength Bulk Metallic Glasses and Their Composites: A Review. *Advanced Engineering Materials*. 2015;17(6):761-80.
- Schuh CA, Hufnagel TC, Ramamurty U. Mechanical behavior of amorphous alloys. *Acta Materialia*. 2007 Jul 1;55(12):4067-109.
- Ashby MF, Greer AL. Metallic glasses as structural materials. *Scripta Materialia*. 2006 Feb 1;54(3):321-6.
- Chen LY, Fu ZD, Zhang GQ, Hao XP, Jiang QK, Wang XD, et al. New class of plastic bulk metallic glass. *Physical review letters*. 2008;100(7):075501.
- Chen LY, Hu HT, Zhang GQ, Jiang JZ. Catching the Ni-based ternary metallic glasses with critical diameter up to 3 mm in Ni-Nb-Zr system. *Journal of alloys and compounds*. 2007;443(1-2):109-13.
- Lin S, Liu D, Zhu Z, Li D, Fu H, Zhuang Y, et al. New Ti-based bulk metallic glasses with exceptional glass forming ability. *Journal of Non-Crystalline Solids*. 2018;502:71-5.
- Wang, Wei-Hua, Chuang Dong, and C. H. Shek. "Bulk metallic glasses." *Materials Science and Engineering: R: Reports* 44, no. 2-3 (2004): 45-89.
- Suryanarayana C, Inoue A. *Bulk metallic glasses*. CRC press; 2017.
- Huang L, Pu C, Fisher RK, Mountain DJ, Gao Y, Liaw PK, et al. A Zr-based bulk metallic glass for future stent applications: Materials properties, finite element modeling, and in vitro human vascular cell response. *Acta biomaterialia*. 2015;25:356-68.
- Li HF, Zheng YF. Recent advances in bulk metallic glasses for biomedical applications. *Acta biomaterialia*. 2016; 36:1-20.
- Gong P, Yao K, Wang X, Shao Y. A New Centimeter-Sized Ti-Based Quaternary Bulk Metallic Glass with Good Mechanical Properties. *Advanced Engineering Materials*. 2013;15(8):691-6.
- Xie KF, Yao KF, Huang TY. A Ti-based bulk glassy alloy with high strength and good glass forming ability. *Intermetallics*. 2010 Oct 1;18(10):1837-41.
- Zhang L, Zhu ZW, Wang AM, Li H, Fu HM, Zhang HW, et al. 2Zr30. 3Cu8. 3Fe4Be21. 2 bulk metallic glass with exceptional glass forming ability and remarkable compressive plasticity. *Journal of alloys and compounds*. 2013; 562:205-10.
- Zhang L, Tang MQ, Zhu ZW, Fu HM, Zhang HW, Wang AM, et al. Compressive plastic metallic glasses with exceptional glass forming ability in the Ti-Zr-Cu-Fe-Be alloy system. *Journal of Alloys and Compounds*. 2015;638:349-55.
- Tang MQ, Zhang HF, Zhu ZE, Fu HM, Wang AM, Li H, et al. TiZr-base bulk metallic glass with over 50 mm in diameter. *Journal of Materials Science & Technology*. 2010 Jun 1;26(6):481-6.
- Singh VP, Tekin HO, Badiger NM, Manici T, Altunsoy EE. Effect of heat treatment on radiation shielding properties of concretes. *Journal of Radiation Protection and Research*. 2018;43(1):20-8.
- Sayyed MI. Investigations of gamma ray and fast neutron shielding properties of tellurite glasses with different oxide compositions. *Canadian journal of physics*. 2016;94(11):1133-7.
- Issa SA, Tekin HO, Erguzel TT, Susoy G. The effective contribution of PbO on nuclear shielding properties of xPbO-(100-x) P 2 O 5 glass system: a broad range investigation. *Applied Physics A*. 2019;125(9):640.
- RSICC Computer Code Collection. MCNP- A General Monte Carlo N-particle Transport Code, Version 5. 2008.
- M.J. Berger, J.H. Hubbel, XCOM: Photon Cross Section Database, Web Version 1.2. Technology, Gaithersburg, M.D 208899, USA, National Institute of Standards and Technology.1987. Available from: <http://physics.nist.gov/xcom>.
- James EM. *Physics for Radiation Protection: A Handbook*. Copyright WILEY- VCH Verlag GmbH and Co. KGaA, Weinheim. 2006.
- Jackson DF, Hawkes DJ. X-ray attenuation coefficients of elements and mixtures. *Physics Reports*. 1981 Apr 1;70(3):169-233.
- El-Mallawany R, Sayyed MI, Dong MG. Comparative shielding properties of some tellurite glasses: Part 2. *Journal of Non-Crystalline Solids*. 2017;474:16-23.
- Trubey DK, Eisenhauer CM, Foderaro A, Gopinath DV, Harima Y, Hubbell JH, et al. Gamma-ray attenuation coefficients and buildup factors for engineering materials. 1991.
- Harima Y, Sakamoto Y, Tanaka S, Kawai M. Validity of the geometric-progression formula in approximating gamma-ray buildup factors. *Nuclear Science and Engineering*. 1986;94(1):24-35.
- Harima Y. An historical review and current status of buildup factor calculations and applications. *Radiation Physics and Chemistry*. 1993;41(4-5):631-72.

31. Olarinoye IO. Photon buildup factors for some tissues and phantom materials for penetration depths up to 100 MFP. *J. Nucl. Res. Dev.* 2017; 13:57-67.
32. Manohara SR, Hanagodimath SM, Gerward L. Energy absorption buildup factors for thermoluminescent dosimetric materials and their tissue equivalence. *Radiation Physics and Chemistry.* 2010;79(5):575-82.
33. Olarinoye IO, Odiaga RI, Paul S. EXABCal: A program for calculating photon exposure and energy absorption buildup factors. *Heliyon.* 2019;5(7):e02017.
34. Sayyed MI. Investigation of shielding parameters for smart polymers. *Chinese journal of physics.* 2016;54(3):408-15.
35. Chilton AB, Shultis JK, Faw RE. *Principles of Radiation Shielding*, Prentice-Hall, Englewood Cliffs, NJ. 1984.
36. Kaplan MF. *Concrete Radiation Shielding*, John Wiley & Sons, New York, USA. 1989.
37. Taylor ML, Smith RL, Dossing F, Franich RD. Robust calculation of effective atomic numbers: The Auto-Zeff software. *Medical physics.* 2012;39(4):1769-78.
38. Glasstone S, Sesonske A. *Nuclear reactor engineering*, third ed. CBS Publishers & Distributors, Shahdara, Delhi, India. 1986.
39. Singh VP, Badiger NM. Investigation on Radiation Shielding Parameters of Nuclear Technology & Radiation Protection. 2014; 29 (2): 149-56.
40. Cevik UĞ, Bacaksiz EM, Damla N, Çelik AK. Effective atomic numbers and electron densities for CdSe and CdTe semiconductors. *Radiation measurements.* 2008;43(8):1437-42.